ON THE FINITE ELEMENT MODELLING OF RC BEAMS SHEAR-STRENGTHENED WITH FRP

G.M. Chen [1] J.F. Chen [2] J.G. Teng [1,*]

1 Department of Civil and Structural Engineering, The Hong Kong Polytechnic University, Hong Kong, China.
2 Institute of Infrastructure and Environment, School of Engineering, The University of Edinburgh, Edinburgh, U.K.
* Corresponding author; Email: cejgteng@polyu.edu.hk; Tel: +852 2766 6012

Abstract:
A significant number of studies have been conducted on the shear strengthening of reinforced concrete (RC) beams with externally bonded fibre reinforced polymer (FRP) reinforcement in the forms of strips, plates or sheets. However, most of these studies have been experimentally based and only a very limited amount of research is available on the numerical modelling of such beams using the finite element (FE) method. The lack of in-depth FE studies is chiefly due to the challenging nature of modelling shear cracking in RC beams and the interfaces between different materials. This paper presents the results of a recent study in which an advanced FE model was employed to investigate the effects of different modelling assumptions for the interfaces between concrete and steel stirrups, between concrete and steel tension bars, and between concrete and FRP on the predicted shear behaviour of RC beams shear-strengthened with FRP. It first outlines the FE model followed by a number of numerical examples to validate it. The effect of varying the bond-slip modelling approach for each interface is then investigated to illustrate its significance. The results presented in this paper show that proper modelling of the bond behaviour of all three types of interfaces is essential in order to accurately simulate the shear behaviour of RC beams shear-strengthened with FRP and that the effects of the assumed bond behaviour of steel stirrups or steel tension bars are very complex and need much further research.

Key words: Reinforced concrete beams, shear, crack band model, FRP, strengthening, bond behaviour, bond modelling, debonding, finite element method.

Research highlights:

1) FE modelling of shear failure of FRP-strengthened RC beams is investigated.
2) Appropriate modelling of FRP-to-concrete bond behaviour is shown to be essential.
3) The bond between steel tension bars and concrete has a significant effect.
4) The effect of bond between steel stirrups and concrete is very complex.

1. INTRODUCTION

Extensive research has been conducted on the application of fibre-reinforced polymer (FRP) composites in the strengthening of reinforced concrete (RC) structures [1-4]. A significant number of existing studies have been concerned with the shear strengthening of RC beams with externally bonded FRP reinforcement in the forms of strips, plates or sheets [5-9]. Most of these studies have been experimentally based [10-17] and only a very limited amount of research is available on the numerical modelling of such beams using the finite element (FE) method (e.g. [18-31]). The lack of in-depth FE studies may be chiefly due to the challenging nature of modelling shear cracking of concrete in RC beams and the interfaces between the different constituent materials including concrete, internal steel reinforcement and external FRP reinforcement.

A detailed review of existing FE studies on the behaviour of RC beams shear-strengthened with FRP conducted in the past decade can be found in [32]. With a few exceptions (e.g. [28, 29]), these studies generally adopted a tension-stiffening model to define the post-cracking behaviour of internally reinforced concrete. However, such an approach is known to be mesh-dependent [33], so the accuracy of the results may be questioned.

The crack pattern of a shear-critical RC beam, either strengthened or un-strengthened, usually features one or several dominant diagonal cracks, with the concrete cracking being highly localized (e.g. [10,11]). Accurate modelling of such localized cracking in concrete is important for modelling the debonding failure of RC beams shear-strengthened with FRP because the interfacial slip between FRP and concrete is directly caused by the localized cracking of concrete [32,34]. However, few studies have been successful in modelling such localised cracking of concrete. Even for those few studies which defined the bond-slip behaviour between FRP and concrete and successfully simulated the FRP debonding failure mode [25, 27-29], the predicted strain distributions in the FRP were still in poor agreement with test results. This may be due to inaccurate predictions of the crack pattern and the localized cracking behaviour of concrete.

For accurate modelling of localised cracking behaviour in RC beams with or without FRP shear reinforcement, it is essential to adopt an appropriate material model to define the post-cracking tensile behaviour of concrete [33]. The bond behaviour between the concrete and the internal steel reinforcement and that between the concrete and the external FRP reinforcement may also play a significant role.

In the present paper, an advanced FE model for RC beams shear-strengthened with FRP [32] is briefly described first. This model takes into appropriate account all the above factors and is developed based on an advanced FE model for intermediate

crack (IC) debonding [34] in which the importance of the accurate modelling of the bond behaviour between tension steel reinforcement and concrete was highlighted in accurate modelling of IC debonding. Several numerical examples are then presented which show that this FE model is capable of accurately modelling the shear failure of RC beams shear-strengthened with FRP in terms of the overall load-displacement response, failure mode, strains in FRP and crack pattern. The effects of different modelling assumptions for the interfaces between concrete and steel stirrups, between concrete and steel tension bars, and between concrete and FRP on the predicted shear behaviour of RC beams shear-strengthened with FRP are then investigated to illustrate their significance and effects.

2. THE PROPOSED FE MODEL

A brief description of the FE model is presented below, outlining the modelling of concrete cracking, steel bars and FRP as well as the bond-slip behaviours between these materials. By taking advantage of symmetry about both the mid-span and mid-width planes, a quarter of the beam is included in the 2-D FE model as a plane stress problem but with the steel bars and the FRP reinforcement (in the form of strips) represented using truss elements. Loading is applied through displacement control and the nonlinear problem is solved using a dynamic solution approach [35] to overcome convergence difficulty commonly encountered in modelling cracking and debonding processes. More details can be found in [32]. The FE model was implemented in ABAQUS [36].

2.1 Crack Models for Concrete

Extensive research has been conducted on the numerical modelling of concrete cracking [33, 37, 38]. Concrete cracking may be modelled using either the discrete crack model or the smeared crack model [32]. The former simulates a crack as a geometrical identity so the discontinuities arising from cracking are physically modelled, whilst the latter model treats cracked concrete as a continuum and captures the deterioration process in cracked concrete through a constitutive relationship. When the discrete crack model is implemented in an FE analysis, the cracks are commonly defined along element boundaries. This inevitably introduces mesh bias [32]. Attempts have been made to resolve this problem by developing FE codes with automatic re-meshing algorithms (e.g. [39-41]), but overcoming computational difficulties associated with topology changes due to re-meshing remains a challenge [38].

Smeared crack models may be divided into two types: the fixed smeared crack model and the rotating smeared crack model. They differ in the assumption made for the direction of crack propagation and in the definition adopted for the shear retention factor. A drawback of the smeared crack model is that it leads to the phenomenon of “strain localization”, leading to zero energy consumption during

crack propagation when the element size approaches zero. As a result, the solution is not mesh-objective. Various localization limiters have been proposed to overcome the mesh non-objectivity problem. One of the successful localization limiters is the crack band model [42], which relates the element size to the constitutive law of the concrete so that the fracture energy is independent of element size. It has been shown by Bazant and Planas [37] that the smeared crack model yields about the same results as the discrete crack model when the crack band model is employed by taking the crack opening displacement w as the cracking strain ε_{cr} accumulated over the width h_c of the crack band in a smeared crack model:

$$w = \int_{h_c} \varepsilon_{cr} dh \tag{1}$$

The crack band model was adopted in this study with its details elucidated below.

2.2 Modelling of Concrete

In this study, the concrete was modelled using the plane stress element CPS4 in ABAQUS [36] incorporating the crack band model for modelling its cracking behaviour. For concrete under uniaxial compression, Saenz's stress-strain relationship [43] was adopted following Chen [44]:

$$\sigma = \frac{\alpha\varepsilon}{1 + \left[\left(\alpha\varepsilon_p/\sigma_p\right) - 2\right]\left(\varepsilon/\varepsilon_p\right) + \left(\varepsilon/\varepsilon_p\right)^2} \tag{2}$$

in which σ and ε are the compressive stress and strain respectively, σ_p and ε_p are respectively the experimentally determined maximum compressive stress and the corresponding strain, and α is an experimentally determined coefficient representing the initial tangent modulus. In this study, α was set to be equal to the elastic modulus of the concrete E_c and its value was estimated from the cylinder compressive strength based on the ACI 318 [45] equation (i.e. $E_c = 4730\sqrt{f_c'}$ in MPa). σ_p and ε_p were set to be equal to the test value of the cylinder compressive strength f_c' and 0.002 respectively.

For concrete under uniaxial tension, the tension-softening curve of Hordijk [46] which was derived from an extensive series of tensile tests of concrete was employed:

$$\frac{\sigma_t}{f_t} = \left[1 + \left(c_1 \frac{w_t}{w_{cr}}\right)^3\right] e^{\left(-c_2 \frac{w_t}{w_{cr}}\right)} - \frac{w_t}{w_{cr}}\left(1 + c_1^3\right) e^{(-c_2)} \tag{3}$$

$$w_{cr} = 5.14 \frac{G_F}{f_t} \tag{4}$$

where w_t is the crack opening displacement, w_{cr} is the crack opening displacement at the complete release of stress or fracture energy, σ_t is the tensile stress normal to the crack direction, f_t is the concrete tensile strength under uniaxial tension, G_F is the fracture energy required to create a stress-free crack over a unit area, and c_1=*3.0* and c_2=*6.93* are constants determined from tensile tests of concrete. If no test data are available, f_t and G_F may be estimated from the following CEB-FIP [47] equations:

$$f_t = 1.4\left(\frac{f_c^{'}-8}{10}\right)^{\frac{2}{3}} \tag{5}$$

$$G_F = (0.0469d_a^2 - 0.5d_a + 26)\left(\frac{f_c^{'}}{10}\right)^{0.7} \tag{6}$$

where d_a is the maximum aggregate size. In the present study, it was assumed that d_a = 20 mm if no test data is provided. Note that in Eq (6), $f_c^{'}$ and d_a are in MPa and mm respectively and G_F has a unit of N/mm [48].

The stress-displacement curve defined by Eqs (3)-(6) can be transformed into a stress-strain curve according to the crack band model as depicted by Eq. (1). In ABAQUS, the crack band width h_c is defined as the characteristic crack length of an element. In this study, Rots' recommendation [49] for estimating crack band widths was adopted. For instance, the characteristic crack length of a plane stress four-node square element with a four point Gaussian integration scheme was taken to be $\sqrt{2}e$, where e is the side length of the element.

In this study, the concrete was assumed to have a Poisson's ratio ν = *0.2* and a dilation angle ψ = 35^o [18]. Numerical results not given in this paper showed that both parameters have little effect on the predicted results if failure is not controlled by compressive crushing of concrete [32].

The following shear retention model was adopted in this study to define the shear resistance degradation of cracked concrete following Rots [49]:

$$\beta = \left(1 - \frac{\varepsilon_{cr}}{\varepsilon_{cr,u}}\right)^n \tag{7}$$

where ε_{cr} is the concrete cracking strain corresponding to w_t in Eq. (3) with their

relationship obtained through Eq. (1), $\varepsilon_{cr,u}$ is the concrete cracking strain at the complete release of stress or fracture energy corresponding to w_{cr}, and n is a coefficient controlling the rate of shear degradation. Although the mechanism for the shear retention of cracked concrete is complicated and depends on many factors such as concrete strength, concrete aggregate size and concrete mix [50,51], for the purpose of this study, the predicted results are reasonably insensitive to n within a range of 2 to 5 as demonstrated later.

Eq. (7) implies that the degradation of shear modulus is mainly affected by the ratio of the normal concrete cracking strain ε_{cr} to the maximum crack strain $\varepsilon_{cr,u}$. It may be noted that the shear resistance degradation may also be affected by shear deformation [52, 53]. However, this study is focused on beams with a shear span-to-depth ratio $s/d \geq 2.5$ which normally fail by shear tension with the development of one or a few dominant diagonal shear cracks. It has been shown [53] that in a shear tension failure, the cracking opening displacement dominates the crack deformation and the effect of the shear deformation is insignificant. When shear compression failure occurs, the effect of shear deformation may become more significant but modelling such a failure is beyond the scope of this study.

2.3 Modelling of Steel and FRP and Their Bond Behaviour

Both the steel and the FRP reinforcements were modelled using truss elements. The steel reinforcement was assumed to be elastic-perfectly plastic and the FRP reinforcement was assumed to be linear elastic brittle.

The bond behaviour between internal steel reinforcement (both longitudinal bars and stirrups) and concrete was modelled using the interfacial element COH2D4 in ABAQUS [36]. In the direction parallel to the steel bar-to-concrete interface, the properties of the interfacial elements were defined using the CEB-FIP bond-slip model [47] (Fig. 1a). It may be noted that the CEB-FIP model specifies the unloading branch, but it was found in this study that the unloading behaviour of the bond-slip model has a very limited effect on the behaviour of the beam including the overall load-displacement response and the local cracking of concrete [32]. Nevertheless, a damage evolution law was defined such that the bond-slip curve unloads linearly through the origin (Fig. 1a). In the direction normal to the interface, it was assumed that there is no relative displacement between the steel reinforcement and the concrete.

The bond behaviour between FRP and concrete was also modelled using the interfacial element COH2D4 in ABAQUS [36]. In the direction parallel to the

interface, the properties of the interfacial elements were determined from the simplified bond-slip model for FRP externally bonded to concrete proposed by Lu et al. [54]. Chen et al. [55] showed that material damage has a considerable effect on the performance of the FRP-to-concrete interface between two adjacent cracks. The larger effect of material damage on an FRP-to-concrete interface than a steel bar-to-concrete interface might be due to the existence of a relatively short effective bond length [6] for the latter. The same damage evolution law as for the steel-to-concrete interface was adopted so that the bond-slip curve unloads linearly through the origin after the interface enters the softening range (Fig. 1b). Normal to the interface, the interfacial elements were assumed to behave linear elastically with the normal stiffness estimated from the stiffness of the adhesive layer. This treatment is based on the observation that the interfacial stress normal to the FRP-to-concrete interface is small and has little effect on debonding failure [32].

3. VERIFICATION OF THE PROPOSED FE MODEL

The FE model described above has been validated against the test results of many RC beams reported in the literature. Details of the simulated specimens can be found in [32]. The simulated specimens include both control (i.e. without FRP strengthening) and strengthened RC beams; and the failure modes of these specimens include shear tension failure (control beams) as well as shear failure due to FRP debonding and shear failure due to FRP rupture (strengthened beams). A comparison between the FE predictions and the test results of four beams, with or without FRP shear strengthening, are presented next as examples to demonstrate the capability of the present FE model in simulating the shear failure of both strengthened beams (failing by FRP debonding) and control beams (shear tension failure). Details of these four beams are summarized in Table 1.

A mesh convergence study reported in [32] showed that for all the specimens modelled, the element size led to little difference in both the overall load-displacement response and the crack pattern at failure when the element size was equal to or smaller than 10 mm for square or nearly square elements. All the numerical results presented in this paper were obtained using the four node square plane stress element with an element size of about 10 mm if not otherwise stated.

3.1 Control and U-jacketed specimens with steel stirrups [10]

Both specimens BS3 (control beam) and BS5 (strengthened beam) tested by Matthys [10] were reinforced with steel stirrups (Table 1). Specimen BS5 was strengthened with three FRP U-jackets in the test shear span. Figs 2a and 2b show the predicted load-displacement curves for beams BS3 and BS5 respectively with n for the shear retention factor varying from 1 to 5 [Eq. (7)]. Clearly the value of n has a significant effect on the post-peak behaviour of both beams but a very small effect on the pre-peak behaviour and the load-carrying capacity when n varies from 2 to

5. The FE ultimate loads are also in close agreement with the test results for *n* values within the range of 2-5. Note that the actual value for n may vary with a number of factors such as the mix design of the concrete as mentioned above, but $n = 5$ seems to lead to predictions close to test results for both specimens with and without FRP shear reinforcements: when $n = 2,3,4,5$, for beam BS3, the predicted shear capacities are 151.6 kN, 150.7 kN, 149.2 kN and 145.8 kN respectively, which are 10.9%, 10.3%, 9.2% and 6.7% higher than the corresponding test value (136.6 kN); for beam BS5, the predicted shear capacities are 174.6 kN, 174.6 kN, 181.8 kN and 177.7 kN respectively, which are 2.7%, 2.7%, 6.9% and 4.5%. higher than the corresponding test value (170 kN). Further numerical results presented in [32] showed that this conclusion is also valid for specimens from other sources examined in this study, including those without steel stirrups. $n = 5$ was thus adopted in all the simulations reported in the remainder of the paper.

The predicted failure modes are shear tension failure for beam BS3 and shear failure due to the debonding of the left and middle FRP U-strips from the beam sides at the peak load for beam BS5; the predicted failure modes are in agreement with the test observations reported by Matthys [10]. The predicted crack patterns for these two beams (Figs 3a and 3b) are also in close agreement with the test results reported in Matthys [10]. It may be noted that the predicted failure mode remains the same for n=2-5, but it can be different when n=1.

Figures 4a-4c show respectively the distributions of FRP strain, interfacial shear stress and interfacial slip over the most critical FRP U-strip (i.e. the middle U-strip). These quantities are shown in these figures for various values of the mid-span displacement (i.e. different load levels), which is referred to as the displacement hereafter for brevity unless otherwise stated. The predicted maximum FRP strain is 10,762 με (Fig. 4a) which is in close agreement with maximum test value of about 9,900με [10]. It is reasonable that the FE analysis predicted a slightly higher maximum strain than the measured value due to various reasons including the following three. Firstly, the FE analysis was solved using a dynamic solution method [32] so amplifications of strains from dynamic effects could be captured; by contrast, such amplifications could not be captured by the static measurement system employed in the tests. Secondly, the discretely located strain gauges are likely to have missed the position of the real maximum strain. Thirdly, a reading from a conventional electrical strain gauge represents the average strain within the gauge length which is lower than the maximum strain in that zone.

Except for the initial stage with the displacement being up to 11.3mm, the maximum strain in the FRP strip always occurs at about 300mm above the beam bottom (Fig. 4a). Note that the FE analysis predicts a crack band around it, between about 320mm and 250mm above the beam bottom. At a displacement of 16.5 mm, FRP debonding initiates at about 250 mm. When the displacement increases to 17.5 mm, further

debonding has occurred at about 320mm. The two debonded zones are indicated by the two regions of constant strain in the FRP (Fig. 4a) and zero interfacial shear stress (Fig. 4b). The critical shear crack eventually forms within the crack band at about 290mm above the beam bottom. Figure 4c shows that the initiation and propagation of debonding of the FRP strip are associated with a large interfacial slip of about 0.33 mm which in turn is caused by the large crack opening displacement of the critical shear crack. Further analyses showed that the vertical crack opening displacement is almost equal to the sum of the magnitudes of the two maximum interfacial slips on the two sides of the critical shear crack and the deformation of FRP within the debonded zone. It may be noted that at the ultimate state with the displacement being 17.1 mm, the critical FRP U-strip has not yet fully debonded. Its complete debonding occurs when the displacement reaches 17.74 mm (Figs 4a-4c).

3.2 Control and U-jacketed specimens without steel stirrups [11]

The next two specimens for comparison were not reinforced with any stirrups (see Table 1). They were specimens SO3-1 (control beam) and SO3-2 (beam strengthened with six U-jackets equally spaced in the test shear span) reported in Khalifa and Nanni [11]. The predicted load-displacement relationships (Fig. 5) are again in close agreement with the test results. Specimen SO3-1 failed by shear tension and specimen SO3-2 failed by FRP debonding [11]. The predicted crack patterns at the ultimate state (Fig. 6) are in agreement with the test observations. Figure 7 shows that the critical shear crack intersects the most critical FRP strip (i.e. third FRP U-jacket from support) at about 200mm above the bottom of the beam, signified by a constant FRP strain (Fig. 7a), a zero interfacial shear stress (Fig. 7b) and a zero interfacial slip with negative values above and positive values below the crack (Fig. 7c). The predicted maximum strain in FRP is 4,950με which is again close to but slightly higher than the maximum test strain of about 4,700 με [11].

The proposed FE model has also been shown to be capable of accurately simulating the FRP rupture failure mode. More details can be found in [32].

4. ROLE OF BOND MODELLING IN PREDICTING THE BEHAVIOUR OF RC BEAMS SHEAR-STRENGTHENED WITH FRP

In this section, the role of bond modelling between FRP and concrete, between tension bars and concrete, as well as between steel stirrups and concrete in predicting the behaviour of RC beams shear-strengthened with FRP is examined. The two strengthened beams discussed above, viz. beams BS5 and SO3-2 are used as reference beams in the discussions that follow.

4.1 Effect of Bond between FRP and Concrete

Using the two reference beams described above, the effect of adopting a different model for the FRP-to-concrete bond is examined here. For reference specimen BS5, the beam was predicted to fail in shear due to FRP rupture when the FRP U-strips were assumed to be perfectly bonded to the concrete (Fig. 8a). The predicted load-carrying capacity is also increased as a result of this perfect bond assumption, but this increase is not a significant amount. The reason is that for this beam, the amount of shear resistance contributed by the FRP is small due to the small amount of FRP used. Figure 8b shows the predicted crack pattern at the ultimate state based on the perfect FRP bond assumption. In comparison with Fig. 3b where the bond between FRP and concrete was properly modelled, the assumed perfect bond leads to the branching of the critical shear crack as seen in Fig. 8b. Note that the curve labelled with 'normal bond for FRP' in Fig. 8a was predicted by modelling the bond between FRP and concrete as described in section 2.4, while the 'perfect bond for FRP' curve was obtained by assuming that the FRP is perfectly bonded to the concrete so no slips occur between them. Similar terminology is used in the rest of this paper.

Specimen SO3-2 was predicted to fail in flexure at a load much higher than the test value when a perfect bond was assumed between the FRP U-strips and the concrete (Fig. 9a). In this FE model, FRP debonding failure is suppressed due to the assumption of perfect bond between concrete and FRP, resulting in a shear capacity that exceeds its flexural capacity. Figure 9b shows that there are multiple diagonal shear cracks at the ultimate state for the beam with perfectly bonded FRP. This contrasts with Fig. 6b where the predicted crack pattern features a single major diagonal shear crack as observed in the test [11] when the bond between FRP and concrete is properly modelled.

It may be noted that it was common to assume that the FRP is perfectly bonded to the substrate concrete in early FE studies of RC beams shear-strengthened with FRP (e.g. [18-21]). The above comparisons clearly confirm the intuitive expectation that the assumption of perfect bond between FRP and concrete leads to over-estimation of the shear capacity of RC beams shear strengthened with FRP U-jackets. They also show that the degree of over-estimation depends on the amount of FRP used and other properties of the beam. Furthermore, without proper modelling of the bond between FRP and concrete, the predicted crack pattern is also likely to be in error.

4.2 Effect of Bond between Steel Tension Bars and Concrete

The effect of the bond behaviour between the longitudinal steel tension bars and the concrete is examined in this sub-section. Specimen BS5 was predicted to fail in shear due to FRP debonding starting from the left FRP U-strip (Fig. 10b) when the steel tension bars were assumed to be perfectly bonded to the concrete. The

predicted load-carrying capacity of the beam with perfectly bonded tension bars is lower than the test value (Fig. 10a). Figure 10b shows the predicted crack pattern at the ultimate state with the perfect bond assumption for the tension bars. In comparison with Fig. 3b where the bond between steel bars and concrete was properly modelled (i.e. normally bonded tension bars), the perfect bond assumption for tension bars results in steeper and more distributed diagonal cracks. As one of these steeper shear cracks becomes the critical shear crack, the shear capacity is reduced (because less FRP strips are intersected by the steeper critical shear crack).

Specimen SO3-2 was predicted to fail in shear due to FRP debonding at a load much higher than the test value when the steel tension bars were assumed to be perfectly bonded to the concrete (Fig. 11a). Although both the beam with normally bonded tension bars and that with perfectly bonded steel tension bars were predicted to fail in the same mode, the failure load of the latter is much higher than the former. This may be explained by examining the crack pattern at the ultimate state as shown in Fig. 11b for the latter and Fig. 6b for the former. It is seen that although the angle of the critical shear crack remains nearly unchanged (in contrast to specimen BS5 as discussed above), perfectly bonded steel tension bars result in many more distributed diagonal cracks (Fig. 11b) than the same bars with normal bond (Fig. 6b) where a single critical shear crack dominates the crack development in the shear span. The more distributed diagonal cracks lead to narrower cracks especially for the critical shear crack at the same mid-span displacement of the beam. As a result, the FRP debonding failure is delayed due to the slower widening of the critical shear crack and the load-carrying capacity of the beam is thus increased. The increased shear capacity of the beam may also be attributed to an increased contribution from the concrete due to narrower cracks associated with the perfect bond assumption for steel tension bars.

From the above discussions, it may be concluded that the bond between the longitudinal steel tension bars and the concrete also has a significant effect on the shear capacity of RC beams shear-strengthened with FRP. An increase of the bond strength between them can either increase or decrease the shear capacity. This effect is thus complex and requires further investigation.

4.3. Effect of Bond between Steel Stirrups and Concrete

The effect of the bond between the steel stirrups and the concrete is examined herein using specimen BS5 as the reference beam. Four bond scenarios are considered, in which the stirrups are assumed to be:

(a) unbonded;
(b) weakly bonded to the concrete, with the bond behaviour being that depicted by the CEB-FIP bond-slip relationship for steel plain bars [47] (see Fig. 1a);
(c) strongly bonded to the concrete, with the bond behaviour being that depicted by the CEB-FIP bond-slip relationship for deformed steel bars [47] (see Fig. 1a);

and

(d) perfectly bonded to the concrete.

For all the above four scenarios, the two ends of the stirrups were assumed to be connected to the compression and tension longitudinal bars respectively. The failure mode predicted by FE analysis is shear failure due to FRP debonding regardless of the assumed bond scenario. Figure12a shows the predicted load-displacement curves for the four scenarios. This figure shows that the predicted ultimate load is the lowest for weakly bonded stirrups, but is similar for the other three scenarios. The assumed bond condition of the stirrups has almost no effect on the predicted load-displacement behaviour until the first main diagonal crack appears at a shear force of about 140kN and a mid-span displacement of about 11 mm. The curves diverge after that (Fig. 12a). These results show that the effects of the bond condition of the stirrups are complex in the sense that there is not a simple relationship between the bond condition and the shear capacity of the beam. The same can be said for the predicted crack pattern at the ultimate state (Figs 12b-12e).

The shear capacity of the beam consists of contributions from the concrete, the internal steel stirrups and the external FRP U-strips at the ultimate state. All these components are directly affected by the crack pattern. The bond condition of the stirrups affects the crack pattern in a complex manner, making it difficult to quantify its effect on each of the components and thus the total shear capacity of the beam.

The reference test specimen had three stirrups and three FRP U-strips within the test shear span (the steel stirrups are at the same locations as the FRP U-strips) (Fig. 12). Figure 13 shows the development of stresses in these stirrups and U-strips at locations intersected by the main diagonal crack. These stresses are minimal before the main diagonal crack appears at a mid-span displacement between 10 to 11mm for all four bond scenarios. The appearance of the main diagonal crack is signified by the abrupt increase of stress in the stirrups and the U-strips (Fig. 13) and the change of slope in the load-displacement curve for all four bond scenarios except that of perfectly bonded stirrups (Fig. 12).

For the case of unbonded stirrups, the main diagonal crack intersects the middle and right stirrups and the middle and right FRP U–strips at a mid-span displacement of about 11mm (Figs 13b,13c,13e,13f) and then intersects the left stirrup and the left FRP U-strip at a mid-span displacement of about 12mm (Figs 13a, 13d). The appearance of the main diagonal crack is signified by a sudden drop of the load on the load-displacement curve at about 11mm in Fig. 12a. The shear force carried by the concrete is reduced when a diagonal crack appears. Part of the force released by the concrete is transferred to the FRP U-strips and the steel stirrups. Because the stirrups are not bonded to the concrete, a wide crack is needed for them to deform sufficiently to resist a significant amount of force. This explains why the force released by the concrete cannot be immediately balanced by the resistance offered by

the FRP U-strips and the steel stirrups, leading to a drop on the load-displacement curve. On the load-displacement curve in Fig. 12a, a second drop occurs when the peak load of the beam is reached at a displacement of about 17mm due to the rapid propagation of the main diagonal crack towards both the loading and supporting positions, leading to the partial local compressive failure of the concrete near the loading point (Fig. 12b). The left and right stirrups reach 70% and 57% of the yield stress respectively whilst the middle stirrup has yielded at this ultimate state. Gradual debonding of the right FRP strip occurs at a displacement of 19.3mm leading to a decrease of the load. This is followed by the complete debonding of the middle FRP strip at 20.7mm and the left FRP strip at 22.6mm, accompanied by an increase of stress in the left stirrup.

For the case of weakly bonded stirrups, the main diagonal crack first intersects the middle stirrup and the middle FRP U-strip at a displacement of about 11mm and then intersects the left and right stirrups and the left and right FRP U-strips almost simultaneously at a displacement of 12.3 mm (Fig. 13). The peak load is reached at this stage. It is important to note that when the peak load is reached the middle stirrup has only reached about 50% of the yield stress and the middle FRP U-strip has only reached a stress which is about half of the maximum stress it experiences during the whole loading process. The stresses in the other stirrups and FRP U-strips are still negligible at the peak load, but they start to develop rapidly thereafter. Clearly, the occurrence of the main diagonal crack results in a more significant drop on the load-displacement curve in this case (Fig. 12a) compared with the case of unbonded stirrups as described above. After the load drop, the load increases by a small amount when the beam is deformed further (as the beam was loaded using displacement control during the analysis). The peak stresses in both the right stirrup and the right FRP U-strip (Figs 13c and 13f) are simultaneously reached at a displacement of 17.3mm where a second, lower peak load is attained. Concrete cracking between the left and the middle stirrups develops rapidly at this stage, leading to a further reduction of the shear force carried by the concrete and the overall load. The stresses in the right stirrup and the right FRP U-strip start to reduce with the load afterwards, but the stresses in the other stirrups and FRP U-strips remain nearly constant (Figs 13a, 13b and 13d) or increase slightly (Fig. 13e) as some of the force released by the concrete is transferred to them. The stress in the middle FRP U-strip peaks at a displacement of 17.7 mm (Fig. 13e). The final failure of the beam is caused by the complete debonding of the left FRP U-strip at a displacement of 18.4 mm.

For the case of strongly bonded stirrups (which is to represent the bond condition of deformed steel bars in the test [10] as mentioned above), the main diagonal crack first intersects the middle and right stirrups and the middle and right FRP U-strips at a displacement of 11mm and then intersects the left stirrup and the left FRP U-strip at a displacement of about 12 mm. The load-displacement curve of this case differs from those of the above cases in that the occurrence of the main diagonal crack is

only reflected by a change of the slope (Fig. 12a) rather than a load drop. This is because the stirrups are better bonded to the concrete so the shear force released by the concrete due to cracking can be almost immediately transferred to the steel stirrups. It is evident that the main diagonal crack is the widest in the middle of the shear span as stresses in the left and right stirrups and the left and right FRP U-strips (Figs 13a, 13c, 13d, 13f) increase rather slowly. The peak load and the peak stresses in the right stirrup and the right FRP U-strip are reached at a displacement of 17.1 mm. The failure is by the complete debonding of the left FRP U-strip at a displacement of 17.71 mm immediately followed by the complete debonding of the middle FRP U-strip at a displacement of 17.74 mm. Both the left and middle stirrups have reached yielding and the stress in the right stirrup has reached about 85% of the yield stress.

For the case of perfectly bonded stirrups, the main diagonal crack first intersects the middle stirrup and the middle FRP U-strip at a displacement of 10mm (Figs 13b and 13e), then the left stirrup and the left FRP U-strip at 13mm (Figs 13a and 13d) and finally the right stirrup and the right FRP U-strip at 13.7mm (Figs 13c and 13f). The occurrence of the main diagonal crack does not produce any visible change in the load-displacement curve (Fig. 12a) because of the assumed perfect bond. It is also evident that the main diagonal crack is the widest in the middle of the shear span as the stresses in the left stirrup and the left FRP U-strip (Figs 13a and 13d) increase rather slowly, and the rapid increase of stresses in the right stirrup and the right FRP U-strip occurs quite late (Figs 13c and 13f). At a displacement of about 14 mm, a secondary diagonal crack in the left half of the shear span has propagated far enough to cross the middle stirrup and the middle FRP U-strip and then joins the main diagonal crack (Fig. 12e). This process leads to a reduction of the stresses in the middle and left stirrups and an increase of the stresses in the FRP U-strips (due to the effect of multiple cracks [56, 57]). The middle FRP U-strip is completely debonded at a displacement of 17mm (Fig. 13e) leading to a small drop of the load (Fig. 12a) and further extension of the main diagonal crack towards both sides. As a result, an increase of stress is observed in the left (Fig. 13d) and right (Fig. 13f) FRP U-strips. The peak load is reached (Fig. 12a) at a displacement of 19.9mm just before the left FRP U-strip is completely debonded from the concrete (Fig. 13d) and the stress in the right FRP U-strip peaks (Fig. 13f). All the three steel stirrups have reached yielding at the ultimate state.

The peak stress reached in the right FRP U-strip is much higher for both scenarios of perfectly bonded stirrups and unbonded stirrups than the other two scenarios because for the former two scenarios (Fig. 13f), the main diagonal crack intersecting the right FRP strip is more developed (Figs 12b and 12e).

In summary, the effect of the bond between the steel stirrups and the concrete is highly complex. The bond condition affects the crack pattern and the process of crack propagation in a complex manner, which in turn affects the development of

stresses in the stirrups and the FRP U-strips. There is not a simple relationship between these aspects for the reference beam examined in this paper. It should also be noted that the stirrup spacing used in the test beam analysed here is approximately equal to the effective depth. The use of such a large spacing is unlikely in practice except for some very old structures. Consequently, the relative contributions of the concrete, steel stirrups, and FRP as well as some of the other observations made are expected to change with stirrup spacing. Further research is required to achieve a better understanding.

5. CONCLUSIONS

This paper has been concerned with several issues in the FE modelling of RC beams shear-strengthened with externally FRP reinforcement. To this end, an advanced FE model is first described and its accuracy demonstrated by comparing its predictions with test results. In this FE model, the behaviour of all three constituent materials of RC beams (i.e. concrete, steel and FRP) and the bond behaviour of both steel and FRP reinforcements are appropriately represented. Using this FE model, a parametric study has been conducted to investigate the effects of different modelling assumptions for the interfaces between steel stirrups and concrete, between steel tension bars and concrete, and between external FRP reinforcement and concrete in the prediction of the shear behaviour of RC beams shear-strengthened with FRP. The following conclusions may be drawn from the results presented in this paper:

a) Appropriate modelling of the bond behaviour between FRP and concrete is essential; assuming a perfect bond between them may greatly over-estimate the shear capacity of the beam;
b) The bond condition between steel tension bars and concrete has a significant effect on the shear capacity of the beam. It affects both the distribution and the angle of diagonal cracks. A stronger bond can either increase the shear capacity of the beam if the number of diagonal cracks is increased but the angle of the main shear crack is not significantly affected, or decrease the shear capacity of the beam if the angle of the main shear crack is increased.
c) The bond condition between steel stirrups and concrete has a highly complex effect. It affects the crack pattern in a complex manner, which in turn affects the development of stresses in steel and FRP shear reinforcements. Again, a stronger bond can either increase or decrease the shear capacity.

Whilst the effects of the bond conditions of steel stirrups or steel tension bars are very complex and need much further research, the chief conclusion from this study is that proper modelling of the bond behaviour of all three types of interfaces is essential in order to accurately simulate the shear behaviour of RC beams shear-strengthened with FRP. Further research is also required to validate the post peak response of beams. To this end, reliable and accurate measurement of post peak

responses in careful tests is desirable.

6. ACKNOWLEDGEMENTS

The authors are grateful for the financial support received from the Research Grants Council of the Hong Kong SAR (Project No: PolyU 5151/03E) and the Innovation and Technology Commission of the Hong Kong SAR Government (Project No: ITS/084/08). They would also like to acknowledge the support from the Scottish Funding Council for the Joint Research Institute between the University of Edinburgh and Heriot-Watt University which forms part of the Edinburgh Research Partnership in Engineering and Mathematics (ERPem).

7. REFERENCES

[1] Teng, J.G., Chen, J.F., Smith, S.T. and Lam, L. *FRP-Strengthened RC Structures*, Chichester, UK: John Wiley and Sons, Inc. 2002

[2] Oehlers, D.J. and Seracino, R. Design of FRP and steel plated RC structures: Retrofitting beams and slabs for strength, stiffness and ductility. Elsevier, UK, 2004.

[3] Bank, L.C. Composites for construction: structural design with FRP materials, John Wiley & Sons, NY, 2006.

[4] Hollaway, L.C. and Teng, J.G. *Strengthening and rehabilitation of civil infrastructures using fibre-reinforced polymer (FRP) composites*, Cambridge, UK: Woodhead Publishing Limited, 2008.

[5] Chen, J.F. and Teng, J.G. "Shear capacity of FRP strengthened RC beams: fibre reinforced polymer rupture", *Journal of Structural Engineering, ASCE*, 2003; 129(5):615-625.

[6] Chen, J.F. and Teng, J.G. "Shear capacity of FRP-strengthened RC beams: FRP debonding", *Construction and Building Materials*, 2003; 17(1):27-41.

[7] Teng, J.G., Lam, L. and Chen, J.F. "Shear Strengthening of RC Beams with FRP Composites", *Progress in Structural Engineering and Materials*, 2004, 6, 173-184.

[8] Bousselham, A. and Chaallal, O. "Shear Strengthening Reinforced Concrete Beams with Fiber-reinforced Polymer: Assessment of Influencing Parameters and Required Research", *ACI Structural Journal*, 2004, 101(2): 219-227.

[9] Bousselham, A. and Chaallal, O. "Mechanisms of Shear Resistance of Concrete Beams Strengthened in Shear with Externally Bonded FRP", *Journal of Composites for Construction*, ASCE, 2008, 12(5):499-512.

[10] Matthys, S. *Structural Behaviour and Design of Concrete Members Strengthened with Externally Bonded FRP Reinforcement*. PhD thesis, University of Ghent, Belgium, 2000.

[11] Khalifa, A. and Nanni, A. "Rehabilitation of Rectangular Simply Supported RC Beams with Shear Deficiencies Using CFRP Composites", *Construction and Building Materials*, 2002, 16, 135–146.

[12] Bousselham, A. and Chaallal, O. “Behaviour of RC T beams strengthened in shear with CFRP: an experimental study”, ACI Structural Journal, 2006, 103(3):339-347.

[13] Carolin, A. and Taljsten, B. “Experimental study of strengthening for increased shear bearing capacity”, *Journal of Composites for Construction*, ASCE, 2005; 9(6): 488-496.

[14] Pellegrino, C. and Modena, C. “Fiber-reinforced polymer shear strengthening of reinforced concrete beams: experimental study and analytical modelling”, *ACI Structural Journal*, 2006; 103(5):720–728.

[15] Monti, G. and Loitta, M.A. “Tests and design equations for FRP-strengthening in shear”, *Construction and Building Materials*, 2007; 21(4):799–809.

[16] Leung, C.K.Y., Chen, Z., Lee, S., Ng, M., Xu, M and Tang, J. “Effect of Size on the failure of geometrically similar concrete beams strengthened in shear with FRP strips”, *Journal of Composites for Construction*, ASCE, 2007;11(5): 487–496.

[17] Teng, J.G., Chen, G.M., Chen, J.F., Rosenboom, O.A. and Lam, L. “Behavior of RC beams shear strengthened with bonded or unbonded FRP wraps”, *Journal of Composites for Construction, ASCE*, 2009; 13(5):394-404.

[18] Kaliakin, V.N., Chajes, M.J. and Januszka, T.F. “Analysis of concrete beams reinforced with externally bonded woven composite fabrics”, *Composites: Part B*, 1996; 27(3-4):235-244.

[19] Arduini, M., Tommaso, A.D. and Nanni, A. “Brittle failure in FRP plate and sheet bonded beam”, *ACI Structural Journal*, 1997; 94(4):363-369.

[20] Vecchio, F.J. and Bucci, F. “Analysis of repaired reinforced concrete structures”, *Journal of Structural Engineering*, ASCE, 1999; 125(6):644-652.

[21] Lee, K., Al-Mahaidi, R. and Taplin, G. “Non-linear finite element modeling of shear-damaged concrete T-beams repaired with CFRP laminates”, *Proceedings, ACUN-2 International Composites Meeting – Composites in the Transportation Industry*, Sydney, February, 2000.

[22] Kachlakev, D., Miller, T., Yim, S., Chansawat, K. and Potisuk, T. *Finite Element Modeling of Reinforced Concrete Structures Strengthened with FRP Laminates*. Final report, SPR 316, 2001, Oregon Department of Transportation.

[23] Wong, R.S.Y. and Vecchio, F.J. “Towards modeling of reinforced concrete members with externally bonded fiber-reinforced polymer composites”, *ACI Structural Journal*, 2003; 1001):47-55.

[24] Santhakumar, R., Chandrasekaran, E. and Dhanaraj, R. “Analysis of retrofitted reinforced concrete shear beams using carbon fiber composite”, *Electronic Journal of Structural Engineering*, 2004; 4:66-74.

[25] Zhang, Z.X., Ye, L.P. and Lu, X.Z. “Finite element analysis of shear behaviour of RC beams strengthened with U-shaped FRP sheets”,. *Engineering Mechanics*, 2005, 22(4):156-162 (in Chinese).

[26] Elyasian, I., Abdoli, N. and Ronagh, H.R. "Evaluation of parameters effective in FRP shear strengthening of RC beams using FE method", *Asian Journal of Civil Engineering (Building and Housing),* 2006; 7(3): 249-257.

[27] Qu, Z., Lu, X.Z., Ye, L.P., Chen, J.F. and Rotter, J.M. "Numerical modeling of FRP shear strengthened RC beams using compression field theory", *Proceedings, Third International Conference on FRP Composites in Civil Engineering (CICE 2006)*, Miami, Florida, USA, 2006; 391-394.

[28] Simth, S.T., Otoom, O.F.A. and Foster, S.J. "Finite element modelling of RC beams strengthened in shear with FRP composites", *Proceeding of the 2nd International fib Congress*, Naples, Italy, 5-8 Jun, 2006.

[29] Otoom, O.F.A., Smith, S.T. and Foster, S.J. "Finite element modeling of FRP shear-strengthened RC beams", *Proceedings, Third International Conference on FRP Composites in Civil Engineering (CICE 2006),* Miami, Florida, USA, 2006;437-440.

[30] Godat, A. Neale, K.A. and Labossiere, P. "Towards modeling FRP shear-strengthened reinforced concrete beams", *Proceedings, Eighth International Symposium on Fiber Reinforced Polymer Reinforcement for Concrete Structures (FRPRCS-8)*, Patras, Greece, July, 2007;16-18.

[31] Godat, A., Neale, K.A. and Labossiere, P. "Numerical modeling of FRP shear-strengthened reinforced concrete beams", *Journal of Composite for Construction*, ASCE, 2007; 11(6):640-649.

[32] Chen, G.M. *Behaviour and strength of RC beams shear-strengthened with externally bonded FRP reinforcement*. PhD thesis, Department of Civil and Structural Engineering, The Hong Kong Polytechnic University, Hong Kong. China, 2010.

[33] ACI.446.3R, *Finite Element Analysis of Fracture in Concrete Structures: State-of-the-Art*, ACI Committee 446, 1997.

[34] Chen, G.M., Teng, J.G. and Chen, J.F. "Finite element modeling of intermediate crack debonding in FRP-plated RC Beams", *Journal of Composite for Construction*, ASCE, in press.

[35] Chen, G.M., Teng, J.G. and Chen, J.F. "Finite element simulation of IC debonding in FRP-plated RC beams: a dynamic approach", *Proceedings, Ninth International Symposium on Fiber Reinforced Polymer Reinforcement for Concrete Structures (FRPRCS-9)*, Sydney, Australia, July 13-15. 2009.

[36] ABAQUS 6.5 (2004). *ABAQUS User's Manual*.

[37] Bazant, Z.P. and Planas, J. *Fracture and Size Effect in Concrete and Other Quasibrittle Materials*, CRC Press, 1998.

[38] de Borst, R., Remmers, J.J.C., Needleman, A. and Abellan, M.A. "Discrete vs smeared crack models for concrete fracture: bridging the gap", *International Journal for Numerical and Analytical Methods in Geomechanics*, 2004; 28(7-8): 583-607.

[39] Yang, Z.J., Chen, J.F. and Proverbs, D. "Finite element modelling of concrete cover separation failure in FRP plated RC beams", *Construction and Building Materials*, 2003, 17(1): 3-13.

[40] Yang, Z. J. and Chen, J.F. "Fully automatic modelling of cohesive discrete crack propagation in concrete beams using local arc-length methods", *International Journal of Solids and Structures*, 2004; 41(3-4):801-826.

[41] Yang, Z.J. and Chen, J.F. "Finite element modelling of multiple cohesive discrete crack propagation in reinforced concrete beams", *Engineering Fracture Mechanics*, 2005, 72(14):2280-2297.

[42] Bazant, Z.P., Oh, B.H. "Crack band theory for fracture of concrete", *Material of Structure*, 1983; 16:155–177.

[43] Saenz, L.P. "Discussion of equation for the stress-strain curve of concrete - by Desayi, P. and Krishan, S.", *ACI Journal*, 1964;61(9):1229-1235.

[44] Chen, W.F. *Plasticity in Reinforced Concrete*, McGraw-Hill, New York, 1982.

[45] ACI 318. *Building Code Requirements for Reinforced Concrete*, American Concrete Institute, Detroit, Michigan, 2002.

[46] Hordijk, D.A. *Local Approach to Fatigue of Concrete*, PhD thesis, Delft University of Technology, 1991.

[47] CEB-FIP, *CEB-FIP Model Code 90*, Thomas Telford Ltd., London, UK, 1993.

[48] Bazant, Z.P. and Becq-Giraudon, E. "Statistical prediction of fracture parameters of concrete and implications for choice of testing standard", *Cement and Concrete Research* 2002; 32(4):529-556.

[49] Rots, J. G., *Computational Modeling of Concrete Fracture*, PhD thesis, Delft University of Technology, 1988.

[50] Maekawa, K., Pimanmas, A. and Okamura, H. *Nonlinear Mechanics of Reinforced Concrere*, Spon Press, Taylor and Francis Group, London and New York, 2003.

[51] Dabbagh, H. and Foster, S.J. "A smeared-fixed crack model for FE analysis of RC membranes incorporating aggregate interlock", *Advances in Structural Engineering*, 2006; 9(1): 91-102.

[52] An, X., Maekawa, K. and Okamura, H. "Numerical simulation of size effect in shear strength of RC beams", *JSCE Journal of Materials, Concrete Structures and Pavements*, 1998; 35(564):372-393.

[53] Sato, Y., Tadokoro, T and Ueda, T. "Diagonal tensile failure mechanism of reinforced concrete beams", Journal of Advanced Concrete Technology, JSCE, 2004; 2(3): 327-341.

[54] Lu, X.Z., Teng, J.G., Ye, L.P. and Jiang, J.J. "Bond-slip models for FRP sheets/plates bonded to concrete", *Engineering Structures*, 2005; 27(6): 920-937.

[55] Chen, G.M., Chen, J.F. and Teng, J.G. "Behavior of FRP-to-concrete interface between two adjacent cracks in FRP-plated concrete members: a numerical investigation", *Proceedings, Asia-Pacific Conference on FRP in Structures (APFIS 2007)*, S.T. Smith (ed.), Hong Kong, 2007;683-687.

[56] Teng, J.G., Yuan, H. and Chen, J.F. "FRP-to-concrete interfaces between two adjacent cracks: theoretical model for debonding failure", *International Journal of Solids and Structures*, 2006; 43(18-19):5750-5778.

[57] Chen, J.F., Yuan, H. and Teng, J.G. “Debonding failure along a softening FRP-to-concrete interface between two adjacent cracks in concrete members”, *Engineering Structures*, 2007, 29(2):259-270.

Table 1 Geometrical and material properties of four test specimens

Source reference		Khalifa and Nanni (2002)		Matthys (2000)	
Specimen		SO3-1	SO3-2	BS3	BS5
Concrete cylinder compressive strength f_c', MPa		27.5	27.5	37.5	36
Beam dimensions	Span L, mm	1830		3800	
	Width b_c, mm	150		200	
	Height h_c, mm	305		450	
	Shear span s, mm	760		1250	
Steel reinforcement	Tension bars	2Y32		6Y20 (in two rows)	
	Yield strength of tension bars f_{yt}, MPa	460		530	
	Compression bars	2Y32 (deformed)		2Y20 (deformed)	
	Yield strength of compression bars f_{yc}, MPa	460		530	
	Stirrups	None		Y6@400 (deformed)	
	Yield strength of stirrups f_{yy}, MPa	Not applicable		560	
	Elastic modulus of all steel bars E_s, GPa	200		200	
FRP reinforcement	Configuration	None	U-strips	None	U-strips
	Nominal (fibre) thickness t_f, mm		0.165		0.111
	Strip width w_f, mm		50		50
	Centre-to-centre spacing s_f, mm		125		400
	Tensile strength f_f, MPa		3790		3500
	Elastic modulus E_f, GPa		228		233

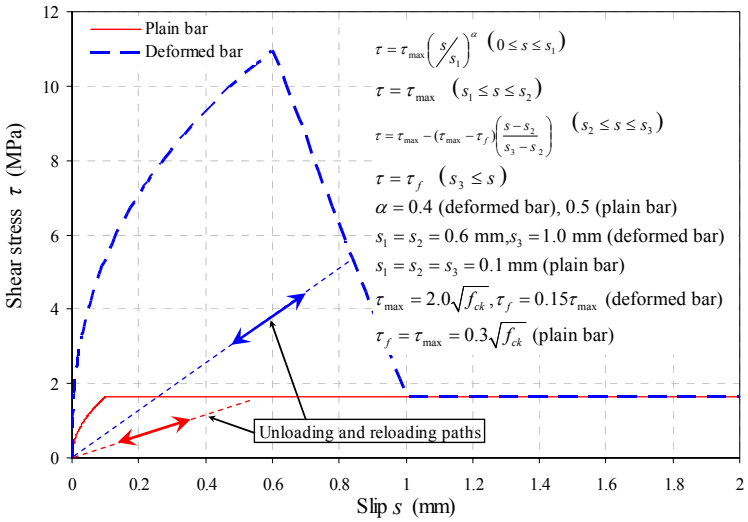

(a) CEB-FIP steel-to-concrete bond slip relationship for f_c' = 30 MPa

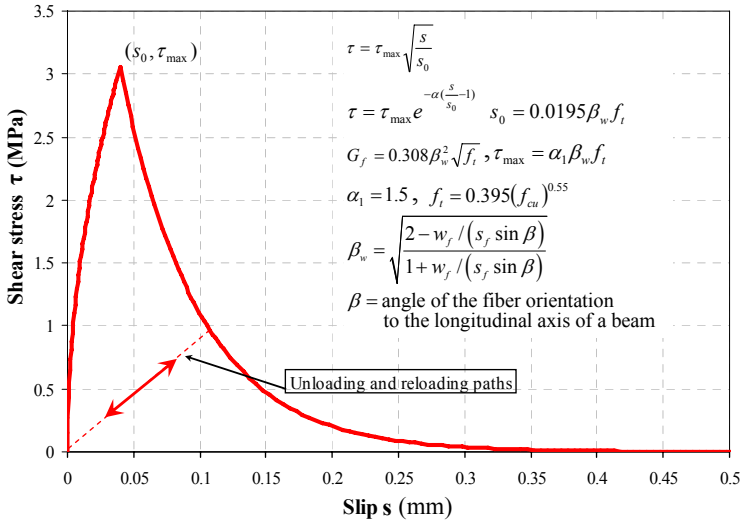

(b) Lu *et al.'s* [54] FRP-to-concrete bond-slip relationship for f_c'=30 MPa and w_f/s_f= 1.0,β = 90o (w_f = FRP strip width; s_f= centre-to-centre spacing of FRP strips as in Chen and Teng [6])

Fig. 1. FRP-to-concrete and steel-to-concrete bond-slip relationships.

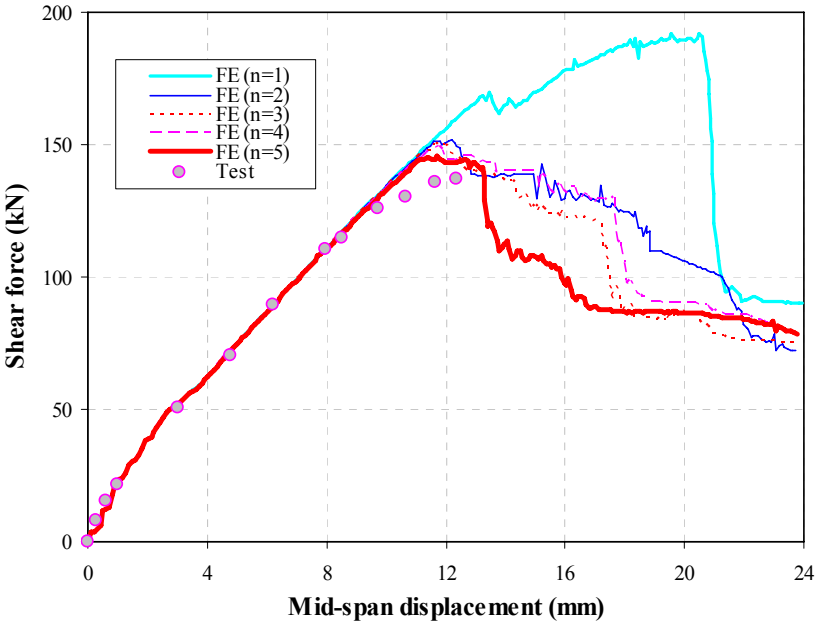

(a) Specimen BS3 (control beam)

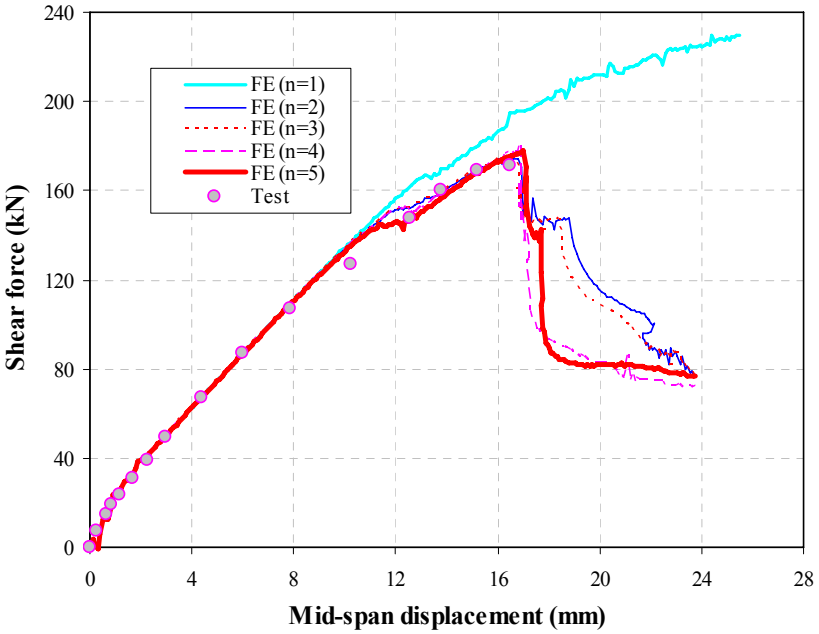

(b) Specimen BS5 (strengthened beam)

Fig. 2. Load-displacement curves for specimens BS3 and BS5.

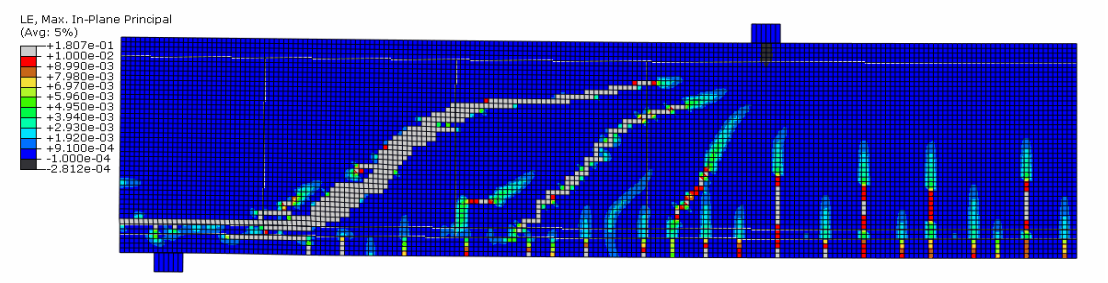

(a) Specimen BS3 (control beam)

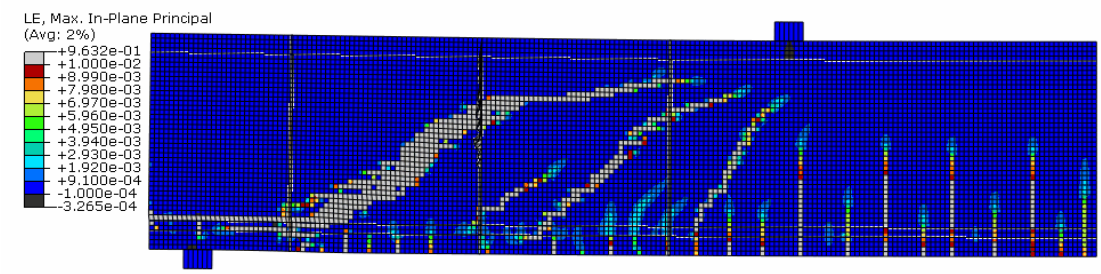

(b) Specimen BS5 (strengthened beam)

Fig. 3. FE crack patterns at ultimate state for specimens BS3 and BS5.

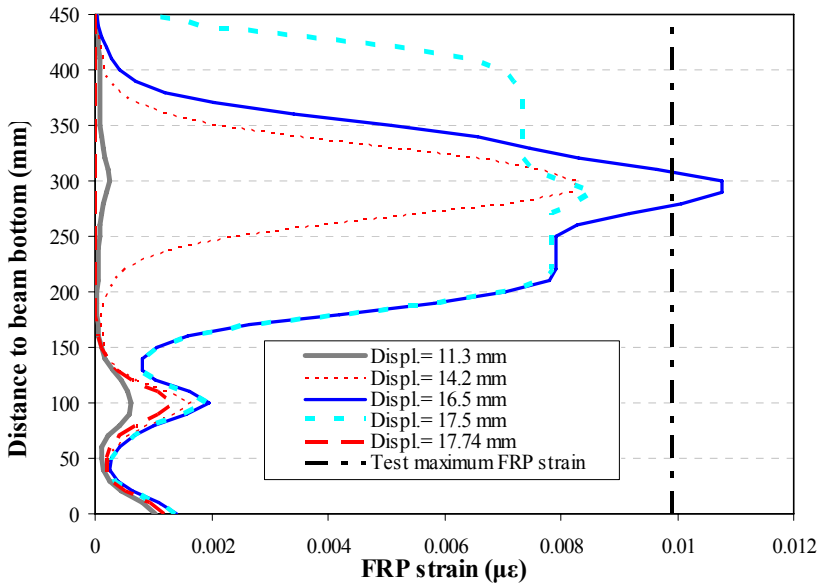

(a) Distribution of strain in FRP

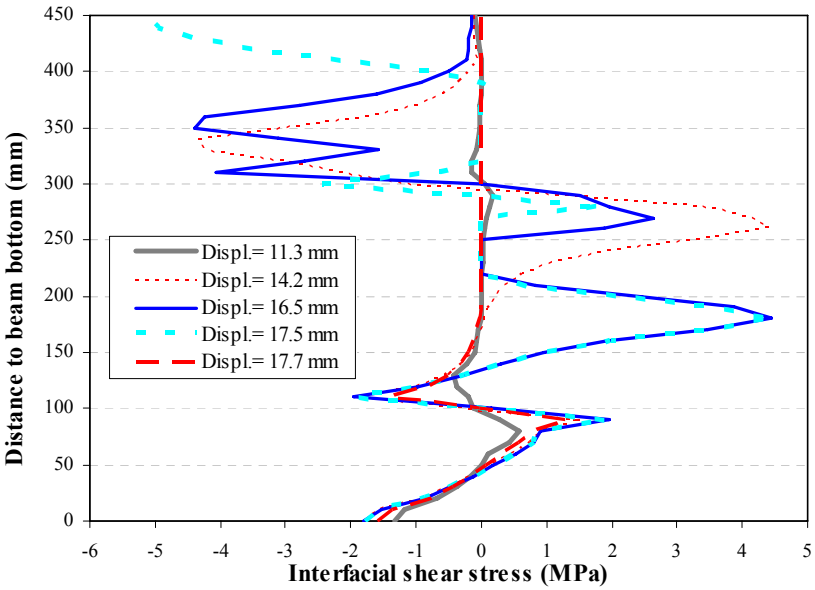

(b) Distribution of interfacial shear stress

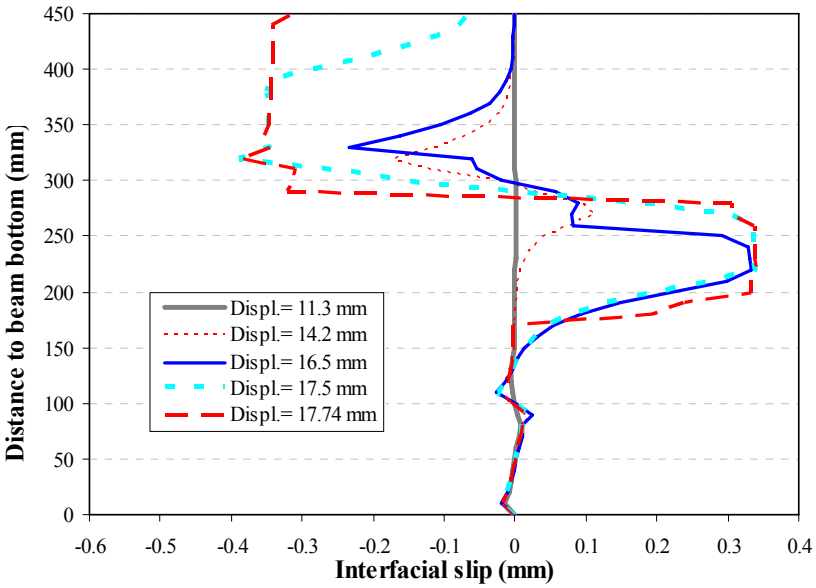

(c) Distribution of interfacial slip

Fig. 4. FE results for the middle FRP U-jacket of specimen BS5.

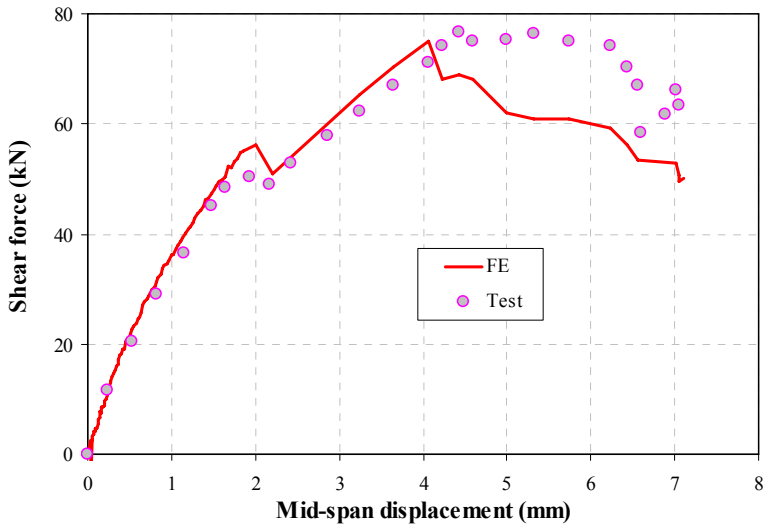

(a) Specimen SO3-1 (control beam)

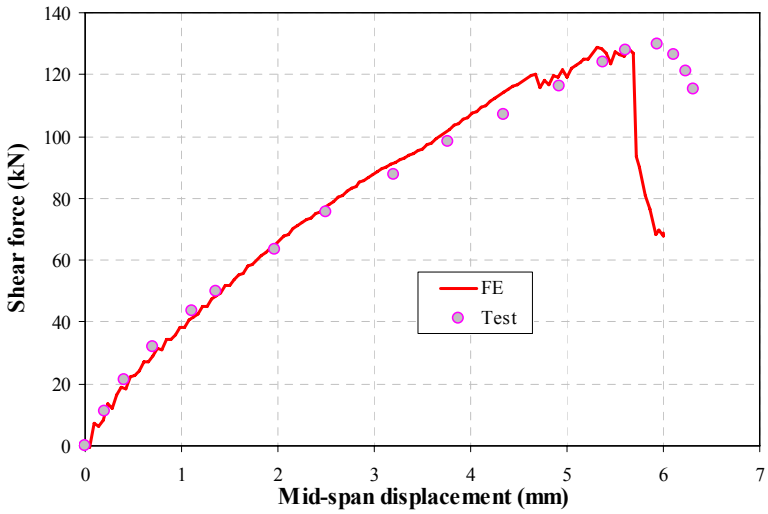

(b) Specimen SO3-2 (strengthened beam)

Fig. 5. Load-displacement curves for specimens SO3-1 and SO3-2.

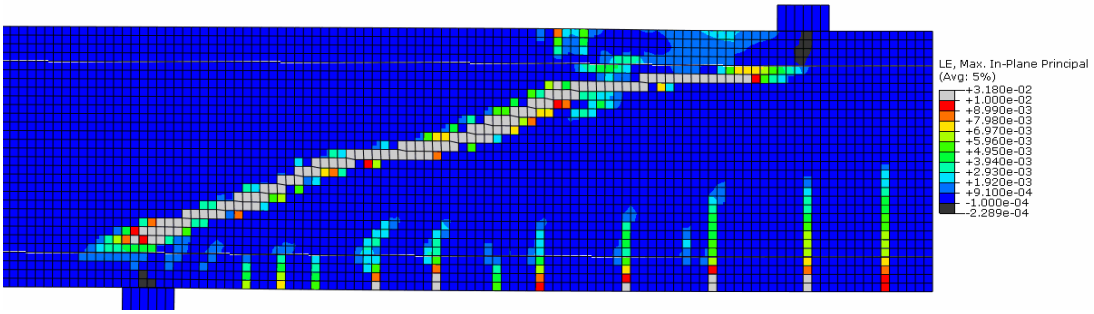

(a) Specimen SO3-1 (control beam)

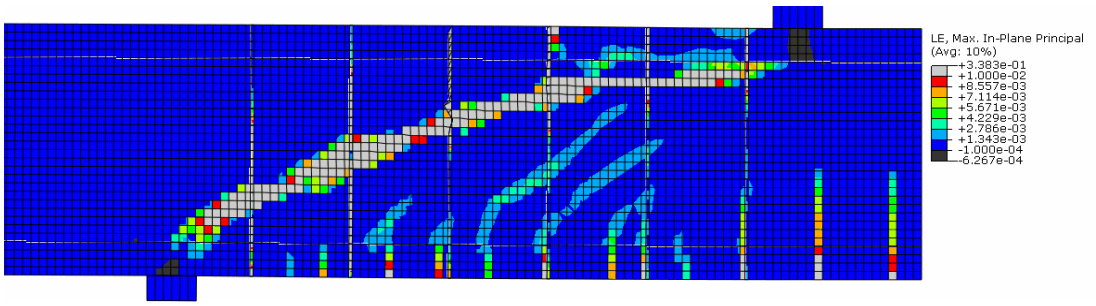

(b) Specimen SO3-2 (strengthened beam)

Fig. 6. FE crack patterns at ultimate state for specimens SO3-1 and SO3-2.

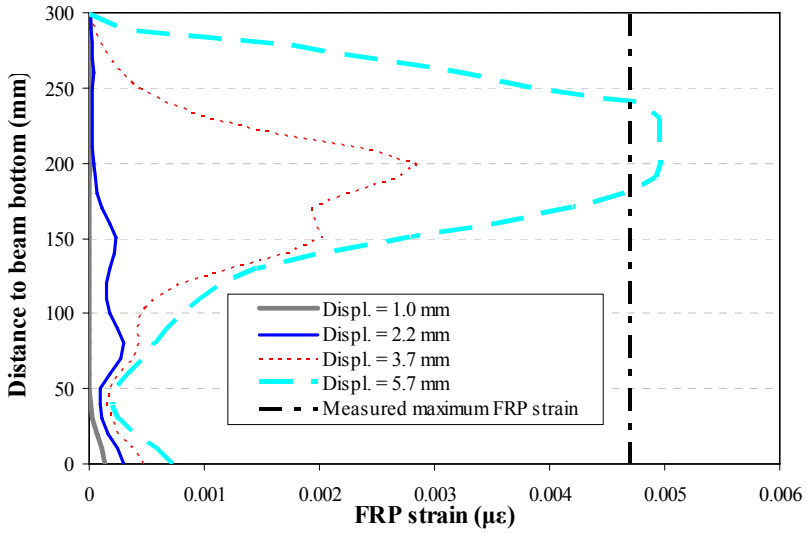

(a) Distribution of strain in FRP

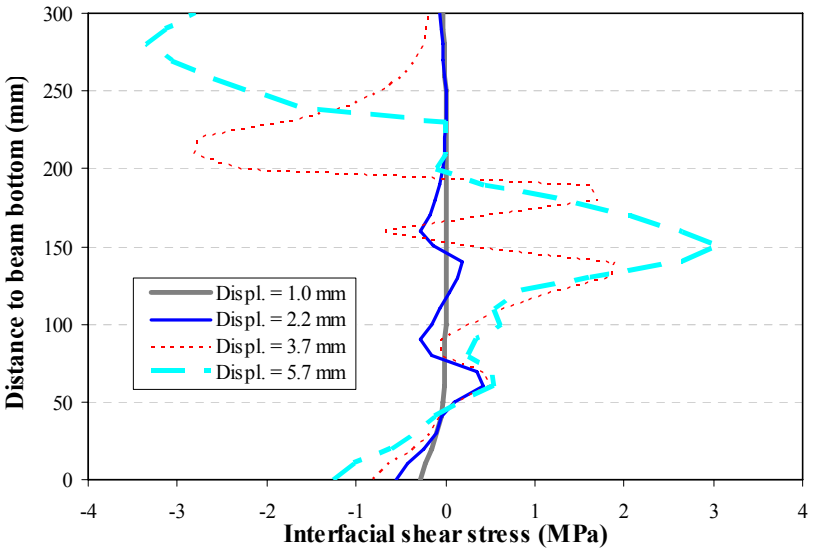

(b) Distribution of interfacial shear stress

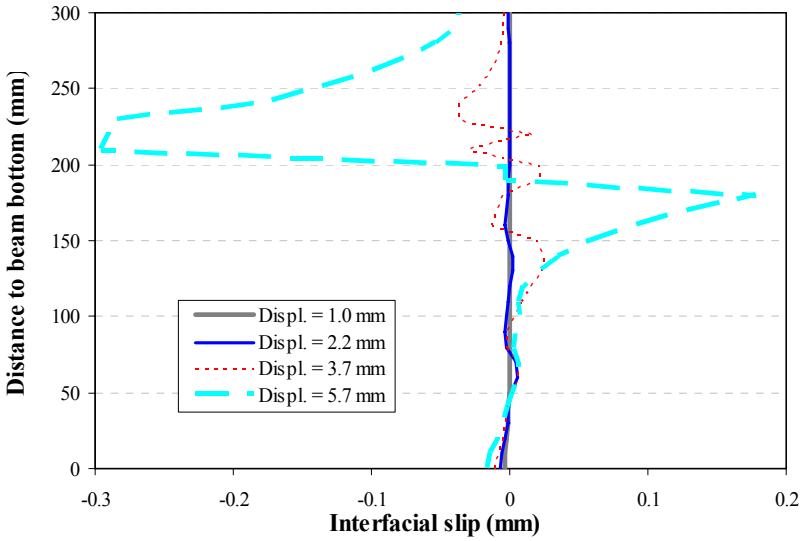

(c) Distribution of interfacial slip

Fig. 7. FE results for the third FRP U-jacket (from support) of specimen SO3-2.

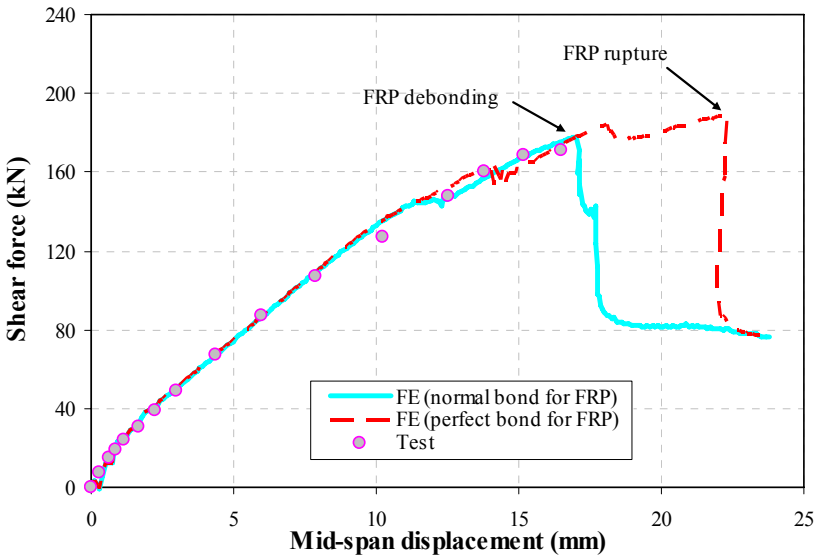

(a) Load-displacement curves

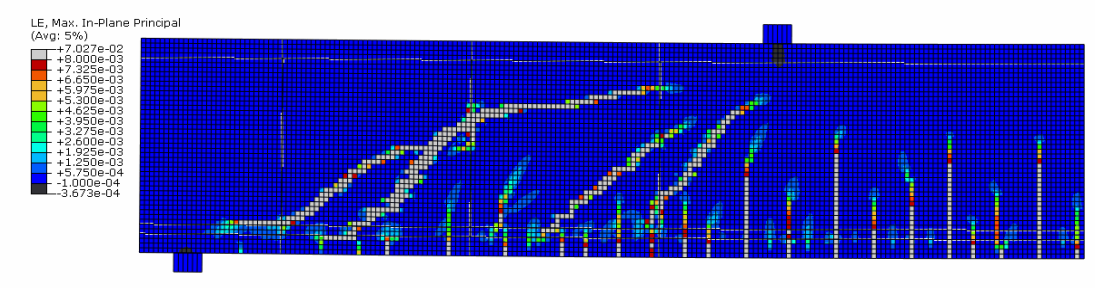

(b) Crack pattern of beam with perfectly bonded FRP

Fig. 8. Effect of bond between FRP and concrete: specimen BS5.

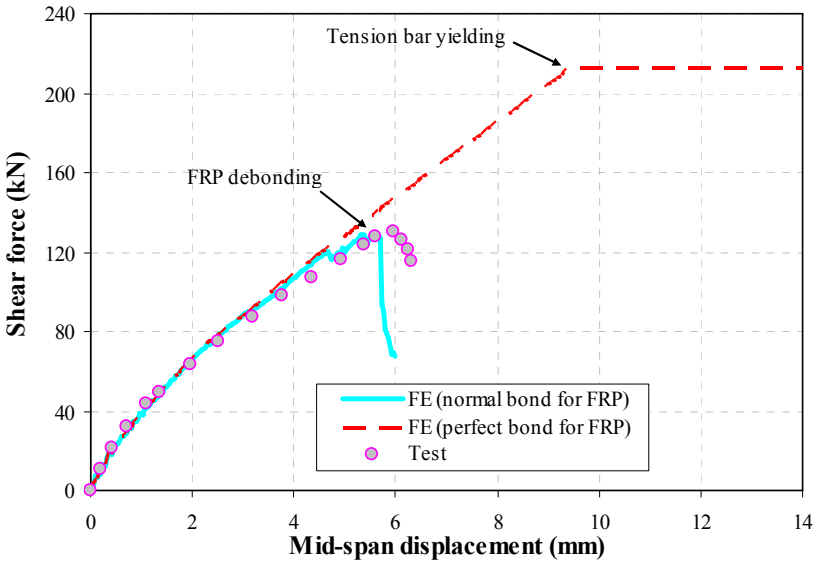

(a) Load-displacement curves

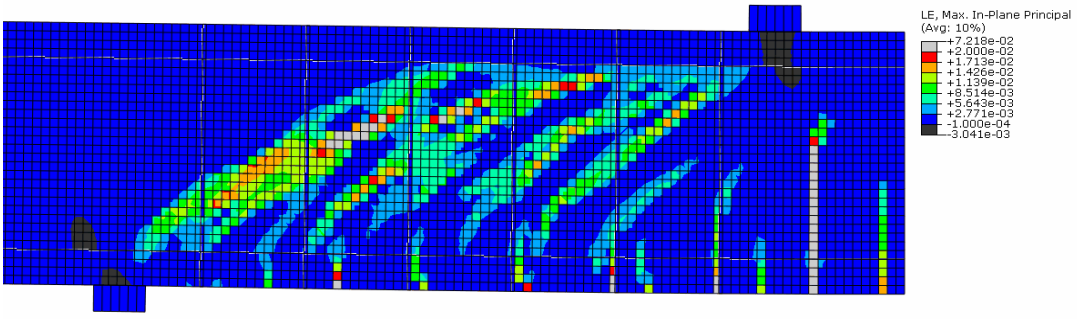

(b) Crack pattern of beam with perfectly bonded FRP

Fig. 9. Effect of bond between FRP and concrete: specimen SO3-2.

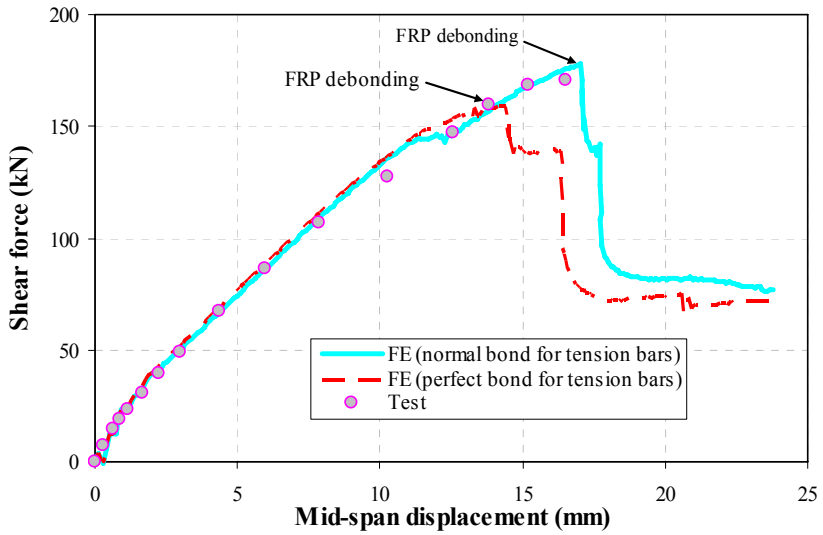

(a) Load-displacement curves

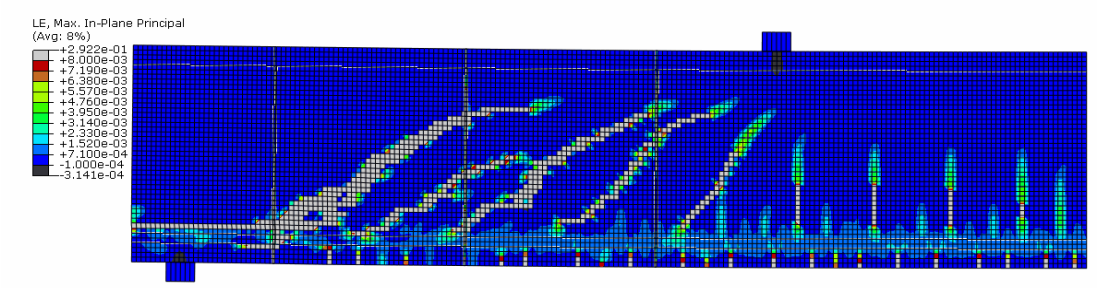

(b) Crack pattern of beam with perfectly bonded steel tension bars

Fig. 10. Effect of bond between steel tension bars and concrete: specimen BS5.

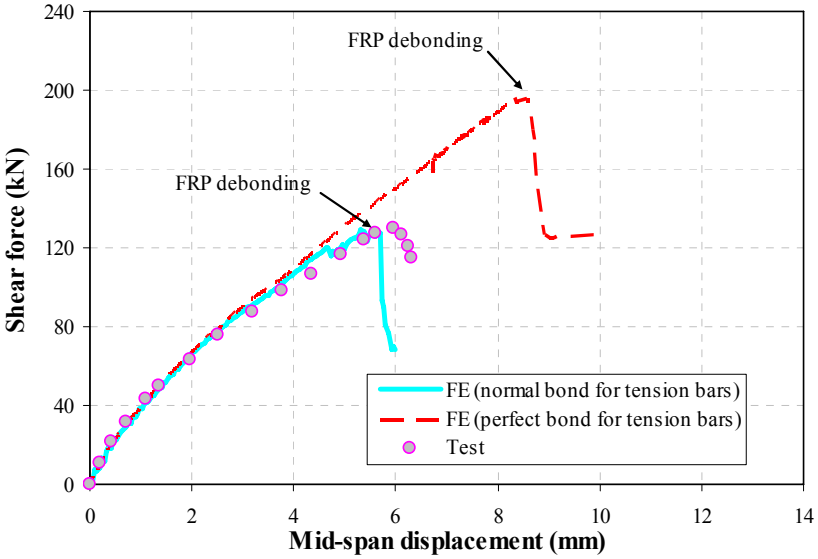

(a) Load-displacement curves

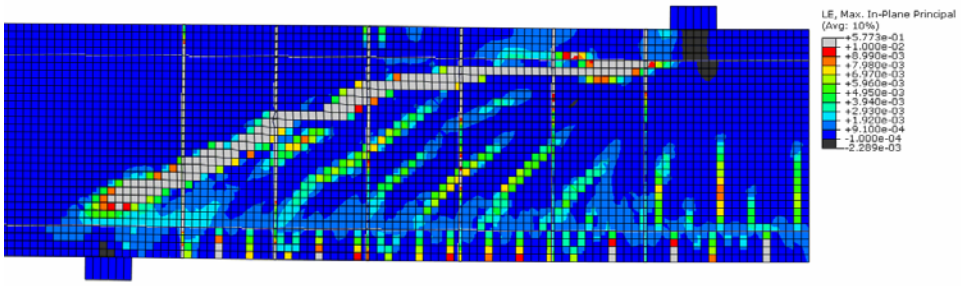

(b) Crack pattern of beam with perfectly bonded steel tension bars

Fig. 11. Effect of bond between steel tension bars and concrete: specimen SO3-2.

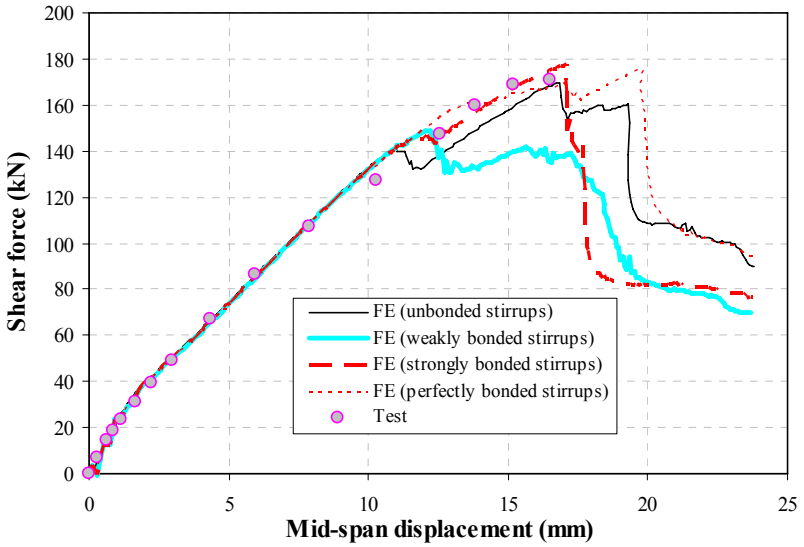

(a) Load-displacement curves

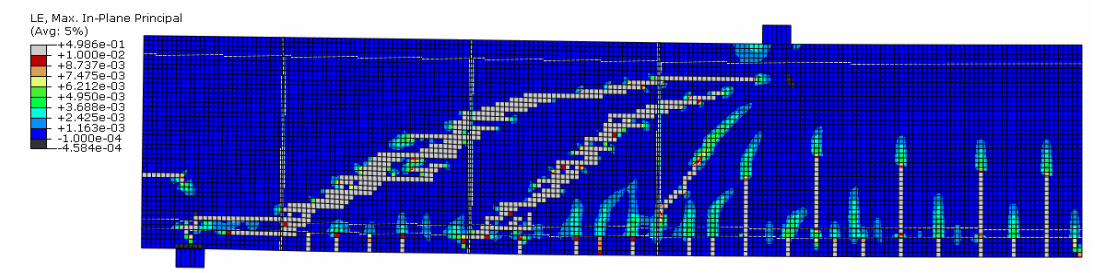

(b) Crack pattern of beam with unbonded stirrups

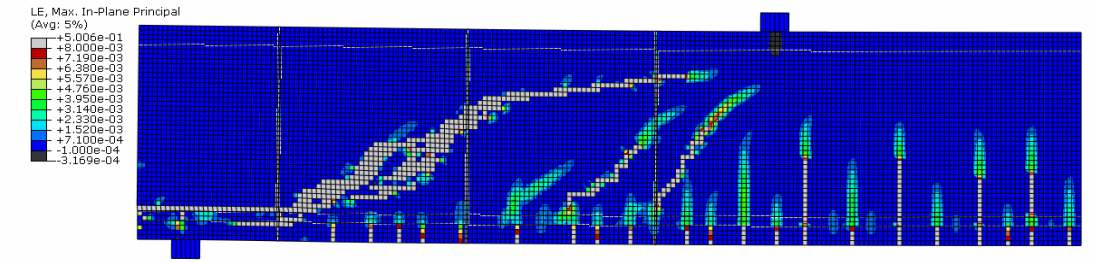

(c) Crack pattern of beam with weakly bonded stirrups

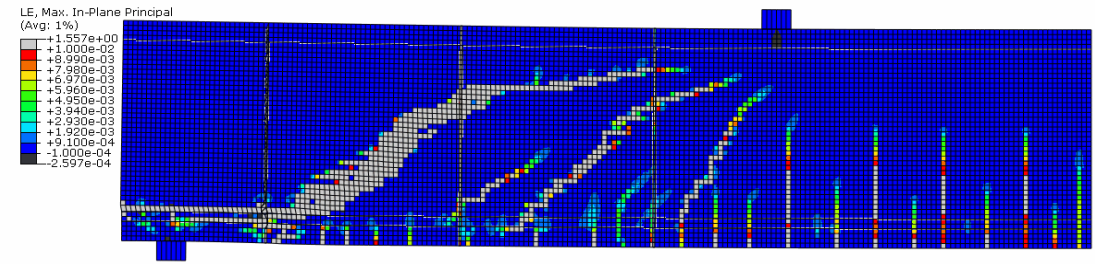

(d) Crack pattern of beam with strongly bonded stirrups

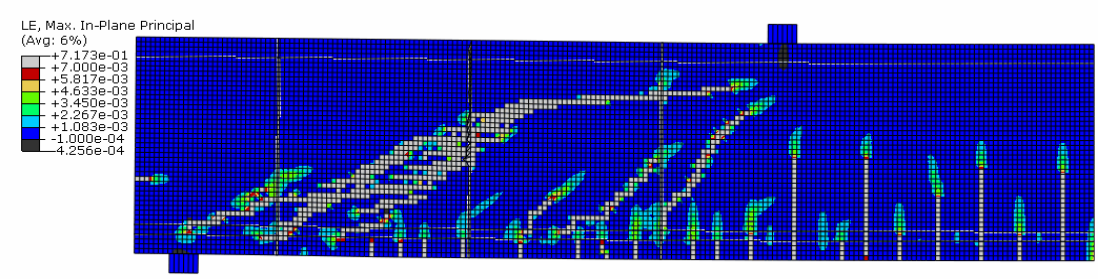

(e) Crack pattern of beam with perfectly bonded stirrups

Fig. 12. Effect of bond between steel stirrups and concrete: specimen BS5.

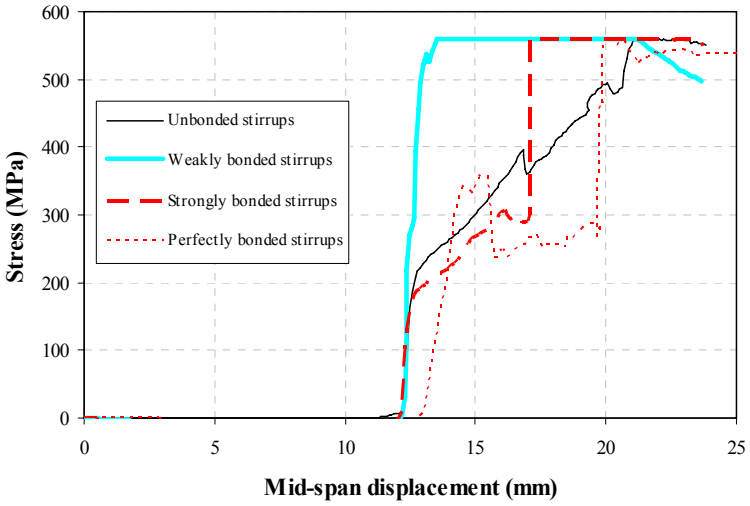

(a) Left stirrup

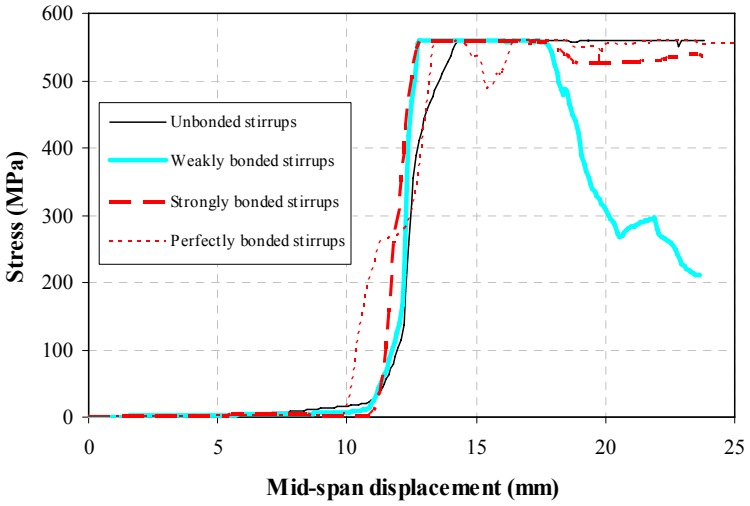

(b) Middle stirrup

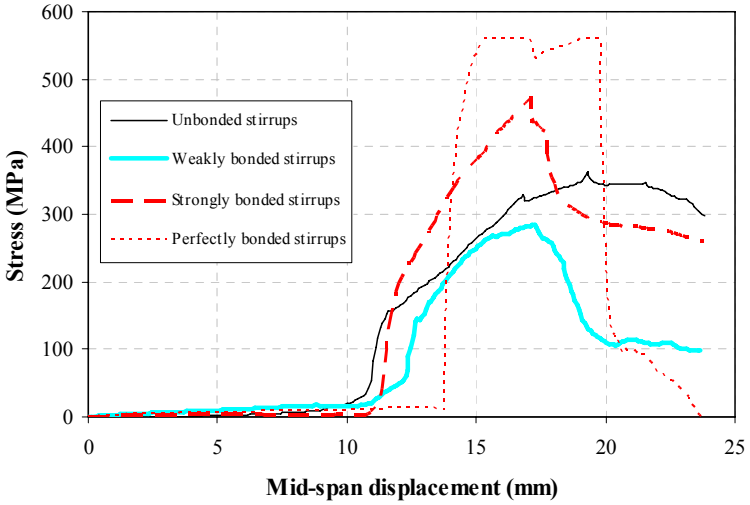

(c) Right stirrup

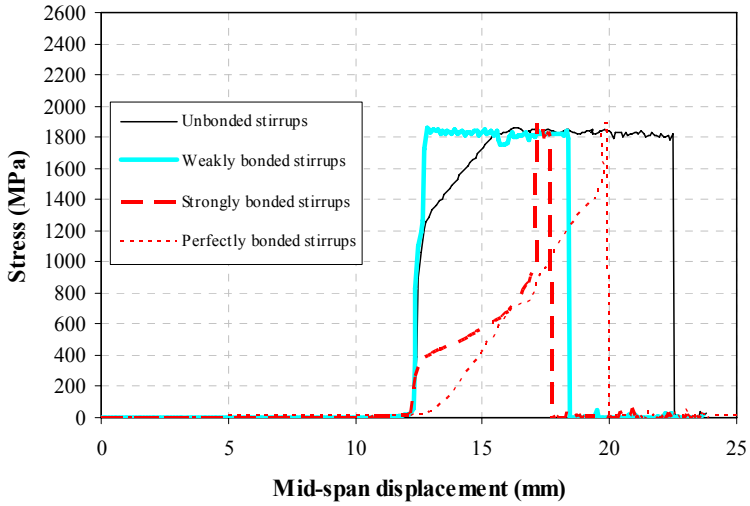

(d) Left FRP U-strip

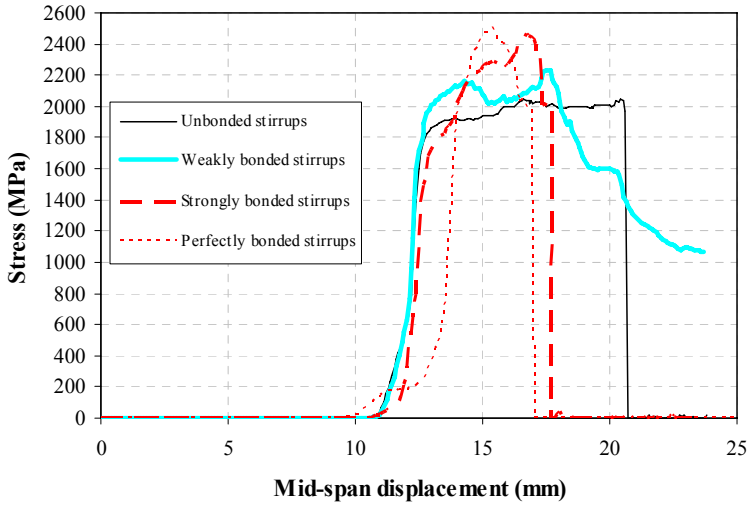

(e) Middle FRP U-strip

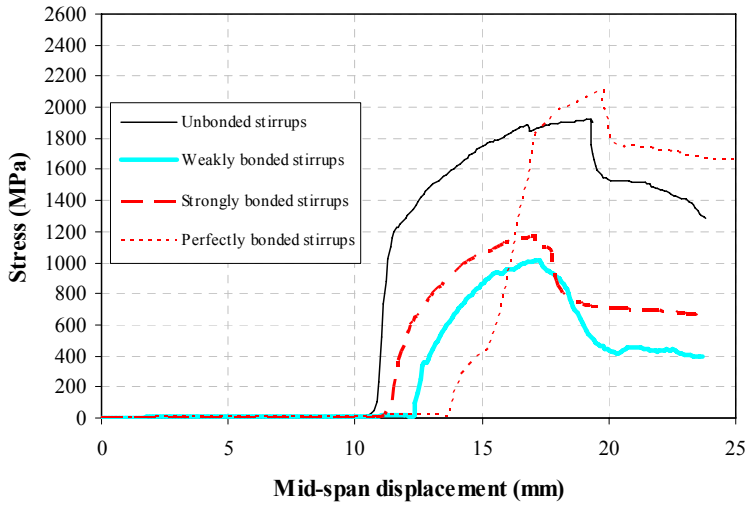

(f) Right FRP U-strip

Fig. 13. Stress development in steel stirrups and FRP U-strips.